Fouling management in oceanic carbon capture via in-situ electrochemical bipolar membrane electrodialysis

Sharifian, R.; van der Wal, H. C.; Wagterveld, R. M.; Vermaas, D. A.

DOI
10.1016/j.cej.2023.141407

Publication date
2023

Document Version
Final published version

Published in
Chemical Engineering Journal

Chemical Engineering Journal 458 (2023) 141407

Contents lists available at ScienceDirect

Chemical Engineering Journal

journal homepage: www.elsevier.com/locate/cej

Fouling management in oceanic carbon capture via *in-situ* electrochemical bipolar membrane electrodialysis

R. Sharifian [a,b], H.C. van der Wal [b], R.M. Wagterveld [b], D.A. Vermaas [a,*]

[a] Faculty of Applied Sciences, Delft University of Technology, Delft, The Netherlands
[b] Wetsus, European Centre of Excellence for Sustainable Water Technology, Leeuwarden, The Netherlands

ARTICLE INFO

Keywords:
Electrochemical
CO_2 capture
Oceanic carbon capture
pH-swing
In-situ mineralization
Bipolar membrane

ABSTRACT

To assist reaching net-zero emissions, the dissolved carbon in the ocean can be extracted to enable an indirect air capture. An electrochemical bipolar membrane electrodialysis (BPMED) is a sustainable method for such capture. The BPMED enables a pH-swing that manipulates the oceanic carbonate-equilibrium using electricity. However, at alkaline-pH, an *in-situ* process suffers from inorganic fouling within the stack, increasing the cost of capture. In the current work, we investigate fouling management strategies including fouling control (i.e., membrane-configuration and current-flow rate optimization) and fouling removal methods. Fouling removal methods including air and CO_2(g) sparging, dissolved CO_2 (aq) cleaning, back-pressure, flow rate increase, and acid-wash are investigated under accelerated fouling conditions. The stack configuration containing the BPM-AEM pairs shows 4 × lower fouling than the BPM-CEM stack, while the carbonate-extraction and faradaic efficiency are similar for both configurations. From the scaling removal methods, only the acid wash combined with the back-pressure removed all the inorganic fouling, recovering both the cell voltage and pressure drop to their initial values. Upon the air sparging, the total cell voltage and pressure drop increased even more due to the trapped gas inside the netted spacers. Cleaning via dissolved and gaseous CO_2 decreases the cell pH, dissolving hydroxide/carbonate-based fouling, but decreases the carbonate-removal significantly which is not preferred. Applying the back-pressure and higher flow rates decelerated the scaling buildup but was not enough to remove the fouling. Using BPM-AEM stacks in combination with periodic acid cleaning has potential as resilient oceanic carbon removal via BPMED.

1. Introduction

To mitigate climate change [1], decarbonisation in all sectors is required, including the water sector [2]. Closing the carbon cycle and decreasing the carbon footprint of the water sector (e.g., desalination plants) are possible through extraction of the oceanic dissolved inorganic carbon (DIC) [3]. An additional benefit is that eliminating the carbonic species prior to membrane based desalination (e.g., reverse osmosis (RO) or electrodialysis (ED)), as a pre-treatment step, can reduce the risk of carbonate-based scaling [4]. Particularly, a pH-gradient based decarbonisation step [5] is advantageous prior to seawater reverse osmosis (SWRO) as low-pH brine stream is ideal for further brine concentration processes [6,7]. The high-pH stream can be returned into the sea, enhancing the atmospheric-carbon absorption in the ocean, and facilitating an indirect air capture. Another benefit of the oceanic-DIC capture is its ability to address decentralized carbon emissions (i.e., ca. 42 % of the total emission) [5].

Oceanic carbon capture is enabled through a pH-swing which provides products of gaseous CO_2(g) (in acidic pH) and/or carbonate minerals (in alkaline pH) [5]. Recently, we have shown the feasibility of the bipolar membrane electrodialysis (BPMED) for electrochemical oceanic carbon capture through *in-situ* alkaline mineralization [3]. The BPM inside the BPMED stack consists of an anion exchange layer laminated/electro-spun to a cation exchange layer, with a water dissociation-catalyst inside the junction layer to enhance the kinetics of the water dissociation [8–10]. Our recent work demonstrated a BPMED containing 10 bipolar-cation membrane (BPM-CEM) cell units to remove the oceanic dissolved inorganic carbon (DIC) in the form of calcium carbonate $CaCO_3$(s) through the *in-situ* alkaline route [3]. However, the fouling inside of the electrochemical stack, particularly the scaling resulting from the alkaline-pH > 9, poses challenges to the technology. To assess the technology's practical feasibility, this work discusses various strategies to control and remove the scaling.

* Corresponding author.
E-mail address: d.a.vermaas@tudelft.nl (D.A. Vermaas).

https://doi.org/10.1016/j.cej.2023.141407
Received 8 September 2022; Received in revised form 15 December 2022; Accepted 9 January 2023
Available online 10 January 2023

Nomenclature

Parameters

ρ	Feed density, kg m^{-3}
μ	Viscosity of feed, kg $m^{-1}s^{-1}$
ε	Spacer porosity, [-] in %
v	Average velocity of the spacer-filled channel, cm s^{-1}
t	Experimental duration between t_0 and t_{end}, s
q	Flow rate in each compartment, ml min^{-1}
l	Length of membrane in vertical axis, m
i	Applied current density, mA cm^{-2}
d	Spacer thickness = intermembrane distance, m
W	Width of each spacer channel, m
V	Total cell voltage, V
R	Membrane resistance, Ω m^2
N	Number of cell pairs (anion and cation exchangemembrane)
I	Applied current, A
F	Faraday constant, s A/mol
A	Membrane active area, m^2
Δp	Pressure difference over acid or base compartments, Pa
OCV	Open circuit voltage, V
Base-pH	pH in the alkaline compartment, [-]
t_r	Cell residence time, s
t_{end}	End of the experiment time, s
t_0	Time of the beginning of the experiment, s
m_{DIC}	Moles of captured $CaCO_3$(s) during the experiment duration, mol
i_{lim}	BPM limiting current density, mA cm^{-2}
d_F	Spacer filament thickness, μm
d_h	Hydraulic diameter of the channel, m
V_{tot}	Total compartment volume (excluding ε), L
V_{sp}	Spacer's volume, L
V_{ini}	Initial cell voltage, V
V_{eff}	Effective compartment volume, L
$S_{v,SP}$	Specific surface of the feed spacer, m^{-1}
Re_h	Hydraulic Reynolds number, [-]
A_{eff}	Cross-section area of the feed channel including the spacer porosity, m^2
$\Delta R_{non-ohmic}$	Difference between the membrane non-ohmic resistance, Ω
ΔR_{Ohmic}	Difference between the membrane ohmic resistance, Ω

Abbreviations

AEM	Anion exchange membrane
AFC	Accelerated fouling conditions
BPM	Bipolar membrane
BPMED	Bipolar membrane electrodialysis
CEM	Cation exchange membrane
DIC	Dissolved inorganic carbon
ED	Electrodialysis
ERS	Electrode rinsing solution
RED	Reverse electrodialysis
RO	Reverse osmosis
SWRO	Seawater reverse osmosis

2. Membrane fouling

There are four types of ion-exchange membrane fouling [11]:

1. Colloidal fouling e.g., clay, precipitated iron, aluminum oxides, and silicates [12]
2. Organic fouling e.g., humic acids [13–17]
3. Inorganic fouling also known as scaling e.g., calcium carbonate ($CaCO_3$) and silica (SiO_2)
4. Biofouling e.g., micro-organisms, extracellular polymeric substances (EPS), and algae [18]

Membrane fouling shortens the lifetime of membranes and decreases the available membrane surface area [11]. Fouling increases the electrical resistance of the membranes, thereby raising the voltage loss and energy required for the process [11,19–22]. Fouling also increases pumping energy needed, by blocking the spacers/compartments, increasing the pressure drop between the inlet and outlet of the electrochemical stack.

Fouling depends on the interaction between feed-compounds and the chemical charged groups on the membrane surface [11]. It is shown in previous studies (on reverse electrodialysis, RED), that the chance of scaling is increased in seawater compartment in the vicinity of the CEM, due to the high concentration of multivalent ions in the seawater (e.g., Ca^{2+} and Mg^{2+}) [20,23–26]. On the other hand, AEM did not show mineral scaling, but is known to be more prone to organic and colloidal fouling especially when combined with fresh water [19,27] (since these compounds are mostly negatively charged). In another study on electrodialysis (ED), it was reported that the membrane scaling formed by Ca^{2+} and Mg^{2+} minerals on AEM surface mostly takes place at neutral pH values, while the CEM was scaled at more alkaline pH [28]. In RED and ED processes, the mineral scaling is always combined with a concentration gradient, thereby inducing uphill transport (i.e., transport from low to high concentrations) of multivalent ions [26,29,30]. However, the lack of such substantial concentration gradient in the BPMED-based carbon capture stack generates a different case, where the impact of the membrane type needs to be studied.

In the BPMED-based *in-situ* mineralization method, when using real seawater as feed, the inorganic fouling in the alkaline pH (≥9) increases the cell voltage drastically [3,31]. Therefore, this work focuses on controlling the inorganic fouling (i.e., scaling), in particular, the carbonates and hydroxide minerals that form at pH between 9 and 12. Considering the low pH in the acidic channels (pH ≤ 4), no mineral scaling is assumed to develop in acidic compartments.

As the fouling is dependent on the cell configuration and the choice of membrane, we first compare the performance of CEM-BPM and AEM-BPM configurations when subjected to a fouling scenario. Other cell configurations including BPM-AEM-AEM [31] or *ex-situ* AEM-BPM-CEM [32] are also possible, but is not considered. Eliminating the third membrane in the cell-units reduces the ohmic resistance in the stack, increasing the $CaCO_3$(s) production per number of membranes, and thus reducing the total stack electrical energy consumption [3]. In addition, we tune the combination of applied current density and residence time to mitigate fouling via process control, and to induce accelerated fouling conditions.

Unfortunately, even by applying control strategies, scaling is inevitable and must be removed physically or chemically. Fouling management strategies include (1) membrane modification, (2) feed pretreatment, (3) membrane cleaning, and (4) changes in the process regime [11]. This work investigates membrane cleaning and changes in the process regime.

The literature review of fouling management in BPMED reveals studies in waste water treatment [33–37] and food industry [38–42]. With research focusing mainly on organic fouling on the AEM [34,37], CEM [35–37,43], and BPM [33,40,41] surfaces. Various methods for fouling removal are reported in literature, including polarity-reversal [44] (not applicable to BPM), reverse flow [45,46], gas sparging [25], cleaning using CO_2-saturated water [19], chemical wash [47], flow rate

increase [48 34] (i.e., Reynolds number [41]), acid–ultrasound cleaning [35], low current density [42], and pulsed electric field (PEF) current mode [41]. For scaling prevention of Ca- and Mg-salts, reducing the feed pH < 3 [28,39] or using pretreatment to remove these ions prior to BPMED [37,49] is suggested the most effective.

While recent previous work demonstrates that BPM-induced carbon mineralization from seawater causes scaling of Ca- and Mg-precipitates [3], no studies have elucidated the most suitable strategy for scaling prevention or removal in this application. Here, we study fouling management strategies to unlock to the potential of carbon capture from seawater via in-situ mineralization. Membrane cleaning methods in this work include air sparging, gaseous CO_2(g) sparging, cleaning using dissolved CO_2 (aq), flow rate increase, back-pressure application, and acid wash (using pure HCl acid or using the produced acid from the BPMED). All cleaning strategies are compared using *in-situ* seawater decarbonization in BPMED under accelerated scaling conditions.

3. Materials and methods

Prior to the experiments, the expected feed and outlet pH, possible minerals, and carbonate removal rate are simulated with Visual MINTEQ Ver. 3.1 at each current density (i) and cell residence time (t_r), following the calculation method presented [3]. The bulk pH is well predicted with this simulation software, including the complexity of pH decreases upon mineral precipitation that takes place *in-situ* [3 10]. The local pH, however, is not reflected in the simulation. Subsequently, experiments for fouling management are conducted.

3.1. Reagents and materials

Fresh synthetic seawater was made by dissolving pure salts in demineralized water, following the procedure in [3], resulting in the same ionic composition shown in Table S1. All reagents were of analytical grade acquired from VWR or Sigma Aldrich. During the experiments, all solutions were kept at ambient lab temperature of 23 °C ± 2 °C. To avoid pre-precipitation in the feed tank, two separate feed tanks were used with their content mixed using *T*-connections just right before entering the electrochemical stack, and not any sooner [3].

The advantage of using synthetic seawater is that biofouling, organic fouling, and colloidal fouling can be excluded (only scaling remains). In real seawater presence of other ions e.g., strontium (Sr^{2+}) and bromide (Br^-) and insoluble matters might influence the type and kinetics of scaling.

Solutions were pumped through the stack by peristaltic pumps (Cole-Parmer, Masterflex L/S Digital drive, USA), through 6.0 mm OD PTFE tubing (EmTechnik). The pH of the feed and outflow streams of the BPMED stack were measured every second, using Orbisit CPS11D-7BA21 pH probes connected to a Liquiline CM444 digital multiparameter transmitter, both from Endress + Hauser, with an accuracy of ± 0.2 pH-units. The pH meters were calibrated weekly. The pressure drop (Δp) between the inlets and outlets of the acidic and alkaline compartments of the stack were measured using two pressure difference transmitters (Endress + Hauser). All membranes used in the BPMED stack were provided by FuMATech B.V. The FBM-130, FKB-PK-130 and FAB-PK-130 were used as bipolar membranes (BPM), cation exchange membranes (CEM) and anion exchange membranes (AEM), respectively, Fig. 1. Electrodes of titanium mesh coated with platinum, provided by MAGNETO Special Anodes B.V. (Schiedam, The Netherlands) were used. The 10 × 10 cm^2 stack is provided by REDstack B.V., with integrated gasket mesh spacers of 400 ± 5 μm (Sefar 07–500/48 PETP netting with an open area of 48 % supplied by AquaBattery B.V.) inserted in between the membranes to act as flow channels. In between each test, the stack (including the membranes and spacers) was cleaned with recirculating HCl acid for several hours, followed by demineralized water and 0.5 M NaCl flush. The stack was opened weekly for inspection.

Two different electrode rinsing solutions (ERS) were tested (Fig. 1):

- 0.25 M $FeCl_2$ + 0.25 M $FeCl_3$ + 1 mM HCl with a conductivity of 71 $mScm^{-1}$ and pH 1–1.5 (with a AEM shielding membrane next to the anode),
- 0.3 M Na_2SO_4, with a conductivity of 38.3 $mScm^{-1}$ and pH of 5–6 (with a CEM shielding membrane next to the anode).

While the water electrolysis requires at least 1.23 V, the iron couple

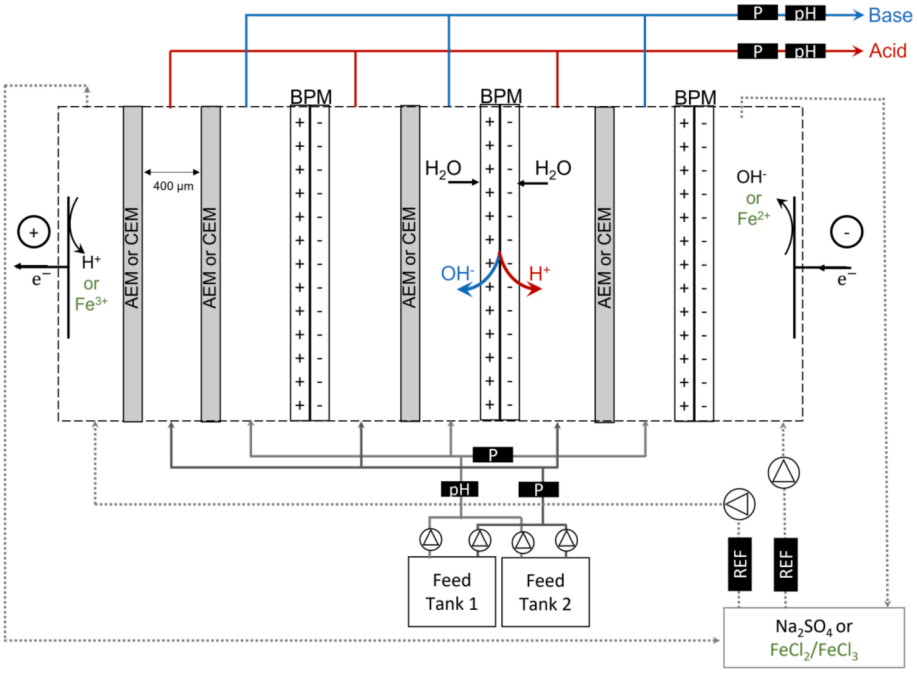

Fig. 1. Schematic representation of the BPMED stack with CEM-BPM (+A/C CBCBCB-) and AEM-BPM (+A/C ABABAB-) configurations. The symbols P, pH, and REF show the pressure difference transmitters, pH sensors, and the Ag/AgCl reference electrode. Feed tank 2 contains $CaCl_2$ and $MgCl_2$ and Feed tank 1 contains remaining salts from Table S1 [3].

is a reversible ERS, requiring 0 V of standard potential thus minimizing the total cell voltage and energy consumption of the process [50]. To exclude the (water) redox voltage from the measurements, two Ag/AgCl reference electrodes were submerged inside of the electrode rinsing solution (ERS) compartments (unless stated). The potentiostat (Ivium Technologies B.V.) measured voltage between the two reference electrodes, excluding the reactions on the electrodes (i.e., the four-electrode connection).

3.2. Experimental procedure

The scaling buildup was measured by inline measurements through monitoring:

1. Pressure difference (Δp_{Base}) development over time, between the inlet and outlet of the base compartments,
2. Development of the total cell-voltage over time,
3. The stack resistance, measured via current interruption (supporting information).

The development of pressure difference (Δp) between the inlet and outlet of the acid compartments over time was also monitored, but stayed constant during all experiments, confirming that no scaling builds up in the acidic compartments. For simplicity, summary of the applied fouling management strategies is given in Table 1, while the supporting information provides a detailed description of each method.

3.3. Accelerated fouling conditions

The accelerated fouling condition is developed by applying a high current density i at each cell residence time t_r, in the single-pass continuous process. Theoretically, at a fixed t_r, the concentration of the BPM-produced OH^- ions increase linearly with i (Figure S5). Subsequently, the increase in the OH^- ions concentration, convert more bicarbonate ions HCO_3^- to carbonate ions. After all carbonates are formed and precipitated, increasing the OH^- ions concentration increases the brucite ($Mg(OH)_2$) precipitation linearly, while carbonates precipitation remains constant, Figure S5. Assuming a linear relationship between the concentration of produced OH^- ions and applied current density i and a linear brucite-production with i (Figure S5), and assuming the crystallization kinetics remain unchanged with a higher current density, the accelerated fouling conditions (AFC) can be defined. AFC suggests that (under the same t_r) running the experiment for 1 hr under $i = 15$ mAcm^{-2} results in the same exposure to mineral precipitation as that of 3 hr under $i = 5$ mAcm^{-2}. To show the relation between the normal and accelerated fouling condition, the voltage buildup graph for the two cases (i.e., flow rates of $q = 24$ and 72 mlmin^{-1}) vs charge density (i.e., OH^- production density) are compared in the SI. After measurements of the removal of DIC, Ca^{2+}, and Mg^{2+} ions and SEM/EDS analysis, it is concluded that carbonate and hydroxide minerals are the main precipitation that take place [3], validating Figure S5.

However, in order to ensure if equal exposure to mineral precipitation results in the same fouling rate and to ensure findings under AFC can be considered as the final solution against scaling in *in-situ* BPMED-based carbon capture, the method of AFC needs to be validated with data from pilots, using real seawater for extended period of time. A combination of redesigned stacks, pre-treatment, additional operational measures, and cleaning procedures might be the way to restrict fouling at minimum cost.

3.4. Data analysis

All the output from the base compartments was captured and stored in sealed storage tanks/bottles for at least 72 h to allow mineral precipitation without the interference of the atmospheric CO_2(g). Thereafter, the sample was filtered through a 0.22 μm (MF-Millipore^{TM}) filter and analyzed on Ca^{2+} and Mg^{2+} concentrations using inductively coupled plasma analysis (ICP). The carbonate concentration in the filtered sample was determined via titration with 0.1 M hydrochloric acid HCl, following the procedure in [3].

3.5. Electrical and pumping energy consumption

The total energy consumption E in Jmol^{-1}$CaCO_3$(s) required for the *in-situ* mineralization is determined using:

$$E = \frac{\int_{t_0}^{t_{end}} V\, I\, dt}{m_{DIC}} + \frac{\int_{t_0}^{t_{end}} (\Delta p_{Acid} + \Delta p_{Base})\, q\, dt}{m_{DIC}} \quad (1)$$

The first part of the equation describes the stack-electrical energy consumption, in which V represents the total cell voltage (V), I the applied current density (A), t the experimental duration between t_0 and t_{end} (s). The second part of the equation describes the pumping energy in which Δp_{Acid} and Δp_{Base} are the pressure drops over the acid- and base compartments (Pa), respectively and q is the flow rate (m^3 s^{-1}), integrated over duration of the experiment. The values are divided by the amount of moles $CaCO_3$ captured during the running time of the experiment (m_{DIC}) [3]. The cell-voltage (V) includes the voltage required

Table 1
Summary of the applied strategies for fouling control (blue) and fouling removal, showing the applied current density i, flow rate per compartment q, and the cell residence time t_r parameters. The reference case and accelerated fouling conditions are also shown. The detailed description of each strategy is given in the supporting information.

Strategy	Configuration	i mAcm^{-2}	q mlmin^{-1}	t_r [s]	Remarks
Reference case	BPM-CEM, BPM-AEM	5	72	2.4	$CaCO_3$(s) is formed but scaling buildup rate is slow
Accelerated fouling	BPM-CEM, BPM-AEM	12.5, 15	24, 72	7.3, 2.4	Scaling buildup rate is fast due to the high OH^- production density
Membrane configuration	BPM-CEM, BPM-AEM	5, 10, 12.5, 15	24,72	7.3, 2.4	Effect of cell-configuration and $i - t_r$ were studied
Air sparging	BPM-CEM	12.5	72	2.4	Air pressure: 1–4 barg, every 10 min (for 5 s), with the first sparge starting 5 min after the start of the experiment
CO_2(g)sparging	BPM-CEM	12.5, 15	72, 24	2.4, 7.3	CO_2(g) pressure: 2 bar or 3 bar, every 5 min, for 5 s or for 3 2 s (combined with backpressure)
Saturated CO_2 (aq)	BPM-AEM	12.5	72	2.4	60 s cleaning after 1 h of experiment (Table S2)
Purge flow	BPM-CEM	12.5	72	2.4	Purge flow (5× and 15× q) every 10 min (for ca. 5 s), starting 5 min after the start of the experiment
Back-pressure	BPM-CEM, BPM-AEM	12.5	72	2.4	Separately or combined with gas sparging and acid-wash, applied by momentarily closing the base-outlet valve
Acid wash	BPM CEM, BPM-AEM	12.5	72	2.4	Diluted HCl (pH 1.5–2) and BPMED-made acid (pH 2.42.6) was used. The effect of acid flow rate was also studied (q = 0, 72, 144 mlmin^{-1}).

for the redox reaction, BPM-water dissociation, and the stack losses including the ohmic and non-ohmic losses [10]. Fouling increases both the ohmic and non-ohmic resistances [11,51].

3.6. Flow velocity and cell residence time

The average flow velocity v (cm s^{-1}) inside the stack is calculated as [52]:

$$v = \frac{q}{60 \times A_{eff}} = \frac{q}{60 \times W \times d \times \varepsilon} \quad (2)$$

where A_{eff} in cm^2 is the cross-section area of the feed channel including the spacer porosity ($\varepsilon \simeq 73$ %, [-]), q the flow rate in the compartment in $mlmin^{-1}$, W width of feed channel (=10 cm for the used electrochemical stack), and d the spacer thickness $\simeq 0.04$ cm. The cell residence time t_r in s is defined as:

$$t_r = \frac{l}{v} \quad (3)$$

where l is the length of feed channel (parallel to the flow direction) = 10 cm and v the average flow velocity v (cms^{-1}) inside the stack. The used flow rate of $q = 72$ and 24 $mlmin^{-1}$ in this work, create flow velocities of v 4.1 and 1.4 cms^{-1}, and t_r of 2.4 s and 7.3 s, respectively.

The hydraulic Reynolds number Re_h as a function of the average velocity of the spacer-filled channel (Equation (2) but in SI unit of ms^{-1}), hydraulic diameter d_h (in m), and W width of feed (in m) can be calculated via [52]:

$$Re_h = \frac{\rho\, v\, d_h}{\mu}, \text{ where } d_h = \frac{4 \times \varepsilon}{\frac{2}{W} + (1+\varepsilon) \times S_{v,SP}} \quad (4)$$

where ρ and μ are the density and viscosity of the feed (synthetic) seawater, respectively (i.e., assumed to be $\rho = 1021.57$ kgm^{-3} and $\mu = 0.000943661$ $kgm^{-1}s^{-1}$). $S_{v,SP}$ is assumed to be $\simeq 18182$ m^{-1} and is the specific surface of the feed spacer [18] (=feed spacer surface divided by its volume, in this work roughly approximated by $\frac{4}{d_F}$ [53], with d_F the spacer filament thickness of 220 μm). Given the above inputs, the Re_h in all experiments stays $Re_h < 1000$ indicating a laminar flow [41].

4. Results and discussion

4.1. Effect of the cell configuration

The AEM-BPM works remarkably better than the CEM-BPM configuration with regards to the magnitude of the scaling buildup (Fig. 2). The cell voltage for the AEM-BPM configuration does not increase with time, while that of the CEM-BPM increases 4× within the same 1.5 h, Fig. 2 (A). The pressure drop curve also shows a substantially better performance of the AEM-BPM configuration compared to CEM-BPM, Fig. 2 (B). Some increase in pressure is observed even for the AEM-BPM case as fouling still does occur. This scaling results in partially blocking the flow path and thus increasing the pressure drop, which is confirmed after opening the stack in both cases, and visually observing the white precipitation on the membranes and spacers surfaces (results not shown). The AEM-BPM initially shows a slightly lower pressure drop (263 vs 430 mbar), which is probably due to a stack-to-stack variability.

As for the DIC removal, both configurations show comparable carbonate removal performances; ca. 79 % ± 8 % for the AEM-BPM and ca. 66 % ± 15 % for the CEM-BPM at the end of experiments. Since the amount of removed carbonate is similar for both cases, and because the CEM-BPM has much higher voltage and pressure drop compared to AEM-BPM, the AEM-BPM is the preferred setup because of its lower energy consumption (Equation (1)). The reason is probably that in CEM-BPM configuration, the fluxes of Mg^{2+} and Ca^{2+} ions towards the base compartment through the CEM (under migration force) create a high concentration of these divalent ions on the CEM boundary layer (i.e., concentration polarization), increasing the saturation index of the carbonate (and hydroxide) minerals close to the surface of the CEM, increasing the (inorganic) fouling rate. We also observed presence of the inner membrane fouling (in form of white precipitates) within the CEM as well as its surface after opening the stack, conform with earlier findings [35]. Such a scenario does not occur in the AEM-BPM configuration, as the AEM suppresses the cation transfer. We hypothesize that this concentration polarization causes inorganic fouling at the CEM surface, in addition to fouling in the spacer channels. This also explains why both the cell voltage and pressure drop increase in the CEM-BPM case, while in the AEM-BPM configuration only Δp increases.

4.2. Effect of the cell residence time and applied current density on scaling buildup

Assuming the thermodynamic equilibrium in the bulk, at base-pH ≥ 9.9, using Visual MINTEQ simulations, >97 % of the dissolved inorganic carbon (DIC) can be removed as calcium carbonate [3]. After that point, any further increase in the OH^- production density ($= \frac{I}{qF} = \frac{It_r}{V_{eff}F}$) only increases the OH^- ions concentration further, accelerating hydroxide containing minerals precipitation, Figure S5. In the experiments, the total cell voltage (Fig. 3) and pressure drop (Figure S6) indeed increase with cell residence time t_r and current density I, showing scaling buildup. The increase of the cell voltage is due to the increase of the membrane ohmic- (Figure S2) and non-ohmic resistances (e.g., explained under section 3.5). In this work, the change in the stack ohmic resistances where much more significant compared to that of non-ohmic resistances, Figure S2 and S3.

Comparing the scaling buildup under accelerated fouling conditions (i.e., q = 24 $mlmin^{-1}$) to that of normal conditions (i.e., q = 72

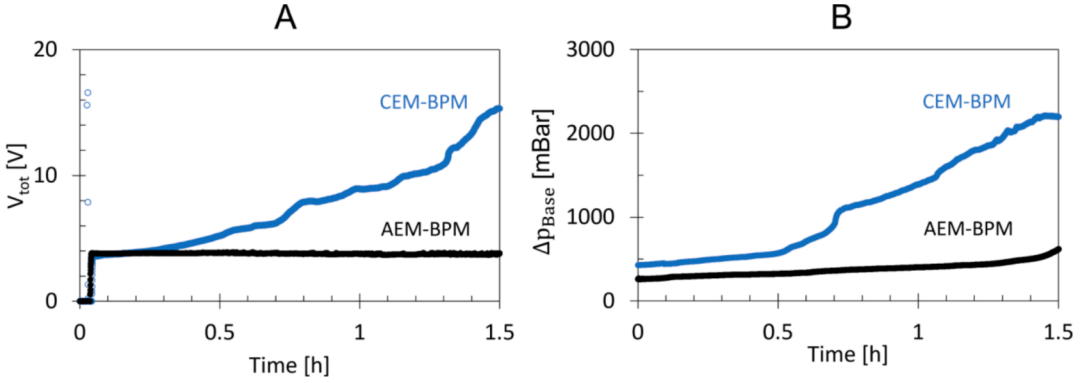

Fig. 2. Comparison of membrane configurations CEM-BPM (+ACBCBCB-) and AEM-BPM (+AABABAB-) under 12.5 $mAcm^{-2}$ and flow rate 72 $mlmin^{-1}$ with regards to the total cell voltage (A) and the pressure drop over the base compartment (B).

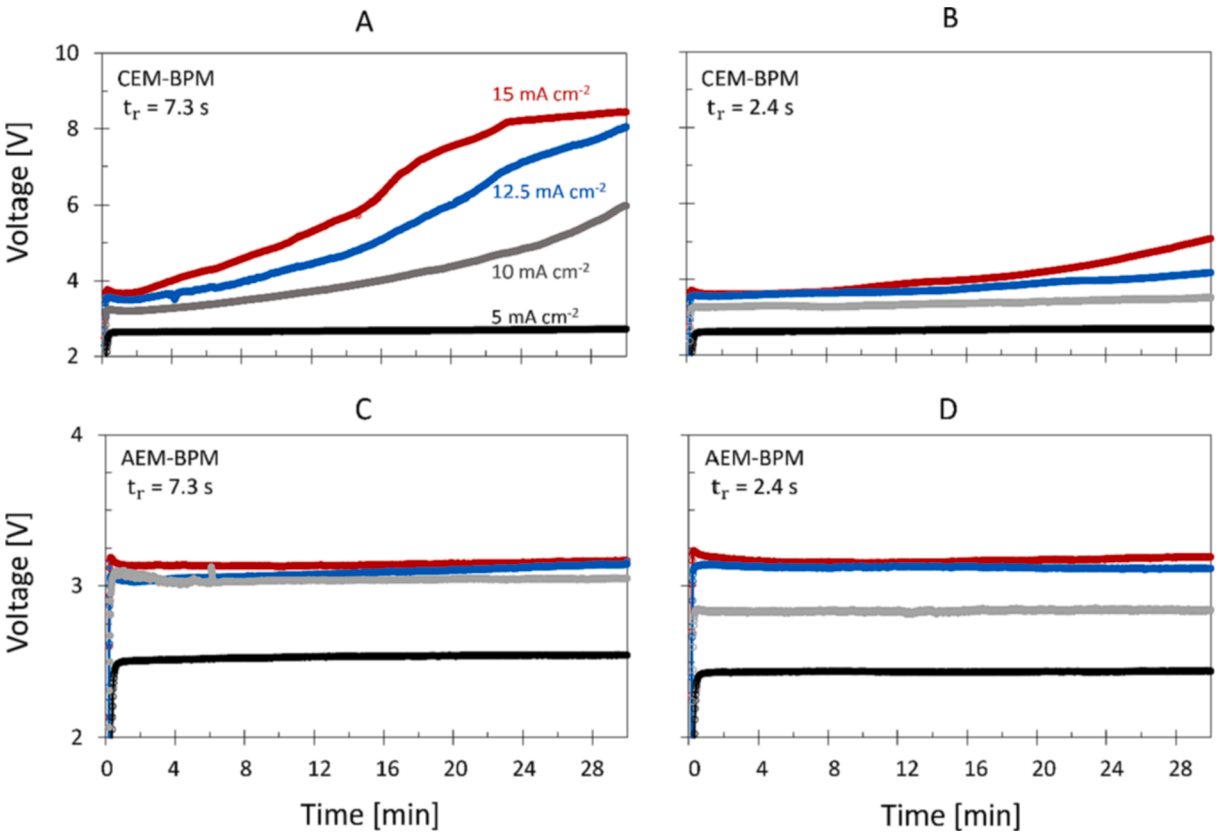

Fig. 3. The measured experimental cell voltage vs time for two cell configurations (A, B: CEM-BPM, and C, D: AEM-BPM), four current densities (red 15, blue 12.5, grey 10, and black 5 mAcm^{-2}) and two cell residence time (t_r = 2.4 and 7.3 s, corresponding to flow rates of 72 and 24 mlmin^{-1} per compartment, respectively).

mlmin^{-1}) show a similar growth rate for the later within the same time frame, Figure S7 and S8.

The cell voltage increases with current density, due to the increase in the ohmic resistances (Fig. 3, voltage of red > blue > grey > black). This can already be seen in different initial voltages between the cases. Furthermore, the cell voltage increases with experiment time due to the mineral precipitations that take place inside of the stack. The increase in the cell voltage vs time due to this scaling buildup is the highest for the CEM-BPM configuration (Fig. 3 (A, B)) due to the concentration polarization of divalent cations close to the surface of the CEM as explained under Fig. 2.

In general, as the cell residence time t_r decreases, the scaling buildup rate decreases, Fig. 3 (B, D) vs (A, C). This is probably because the higher shear force associated with the higher flow rate, mechanically removes the fouling particles better [54–57] and/or because a lower base-pH decelerates scaling buildup. In wastewater treatment via BPMED, the membrane organic fouling is also reported to decrease upon a higher flow velocity because of destabilization of the fouling layer and the concentration polarization layer at higher flow rates [34].

A lower t_r is thus preferred, as long as the base-pH requirement is met for the bicarbonate to carbonate conversion and carbonate precipitation [3]. The measured/simulated base-pH for each experiment shown in Fig. 3 is very comparable and all at pH > 9.9. The OH^- production density associated with each $i - t_r$ is shown in Table S4.

A higher current density creates a higher base-pH and promotes the mineral precipitation inside of the stack (including a higher hydroxide/magnesium containing minerals precipitation, Figure S5). This increases the scaling buildup (Fig. 3 from red to black lines) which is undesired. The lowest current density of 5 mAcm^{-2} does not create much fouling regardless of t_r and cell configuration (Fig. 3, black lines). A low current density also has the added benefit of causing lower ohmic losses (iR), decreasing the total cell voltage and eventually the electrical energy consumption (Equation (1)). Application of a low current density is also reported beneficial to prevent organic fouling in BPMED used in food industry [42].

From Fig. 2 to Fig. 3 it becomes evident that the AEM-BPM cell configuration, in combination with high flow rate and current density of 5–10 mAcm^{-2} (i.e., OH^- production density < 0.01 molL^{-1}, Table S4) provides the best process setting to decelerate scaling buildup. However, despite the decelerated scaling buildup explained above, scaling is inevitable when *in-situ* mineralization is initiated. The stack pressure drop-increase vs time graphs clearly reveals the presence of scaling in all cases, Figure S6. As the fouling is inevitable even under controlled fouling strategies, fouling removal techniques are required. The performance of each cleaning method is discussed below.

4.3. Air sparging

Air sparging under 1 barg injection pressure was not sufficient as gas bubbles got trapped inside of the stack, Fig. 4. The air sparging experiments show a similar trend for voltage and Δp_{Base}, increasing with time, just as the reference experiment (Fig. 4). This suggests that the air sparging did not clean the BPMED stack-base compartments. Not only does the air sparging not recover the cell voltage/pressure drop, but it also even increases them slightly after each injection (Fig. 4 (A, B)-spikes and the slightly higher value after each spike). Such increase is probably due to the presence of stagnant bubbles that are remained trapped in the stack after every air injection. The trapped gas is reported to increase the stack resistance in prior studies [19] as air has much lower electrical conductivity than the feed synthetic seawater (i.e., ca. 10^{-14} [58] vs ca. 5 Sm^{-1}). At the end of each air injection, an effort was made to remove stagnant bubbles from the stack by applying back-pressure through closing a valve located on the outflow of the base compartments (creating pressure buildup of 2–3 bar), but no decrease in the voltage nor

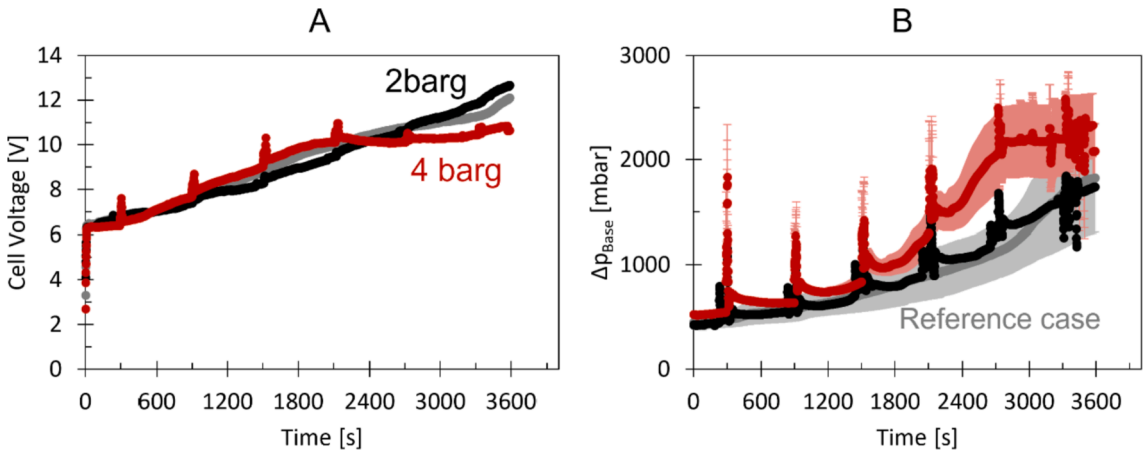

Fig. 4. Air sparging under 2 (black) and 4 barg (red) done for the BPM-CEM configuration (i = 12.5 mAcm^{-2} q = 72 mlmin^{-1}), every 10 min for 5 s, with the reference experiment (i.e., no sparging applied) shown in grey. (A) Cell total voltage and (B) pressure drop over the base compartments vs time. Each set experiment is done three times. The graphs show the average of three repetitions. In (B), the standard errors (=standard deviation/square root of 3) for the reference experiment (light grey) and the 4 barg experiment (in pink) are shown, the case of 2 barg (black) has a standard error of ca. 42 mbar. For (A), the standard error is ca. 0.7–0.9 V for all lines. The spikes in cell voltage and pressure drop are caused by the gas bubbles inside the stack (decreasing conductivity and increasing flow, thus differential pressure).

Δp_{Base} was achieved.

Increasing the air pressure from 2 to 4 barg does not improve the cleaning efficiency (Fig. 4), probably due to the formation of channels between the spacer material (Figure S13). Upon formation of such channels, the air chooses the 'way of least resistance' and only sparges the channels but not the rest of the compartment, particularly the edges and corners. However, air sparging has been shown effective in reverse electrodialysis (RED) where the use of profiled membranes made spacers obsolete [20], suggesting the important role of the spacers in fouling removal strategies.

As a final attempt for sparging in the spacer-filled channels, a pulsed injection was applied, as literature suggests an extra shear force can push out the deposited fouling [19]. Therefore, sparging 3× 2 s (i.e., pulse injection) instead of 1× 5 s (Fig. 4) was applied. However, still no improvement in the efficiency of the cleaning removal is seen, Figure S10.

4.4. Cleaning with carbon dioxide

Sparging of gaseous carbon dioxide is reported to be more effective in scaling removal compared to the air sparging [19]. Gaseous CO_2(g) has the benefit of lowering feed-pH (upon CO_2 dissolution) and thus dissolving carbonate and hydroxide minerals, chemically. The effectiveness of gaseous CO_2(g) sparging in fouling removal is evaluated for 1× 30 s (Figure S9) and 3× 2 s sparging modes, Fig. 5.

The total cell voltage and Δp_{Base} both increase for the reference experiment as expected, Fig. 5- grey line. Logically, this increase is higher under the accelerated fouling condition of Figure S9 compared to Fig. 5. Here, the higher scaling buildup is a result of 3.75× higher concentration of the BPM-produced OH^- ions in the base compartment, which increases the precipitation rate of hydroxide containing minerals (particularly $Mg(OH)_2$). For the reference experiment, the base-pH remains around pH 10 (Fig. 5 (C)) due to the *in-situ* mineralization that takes place inside of the base compartments of the stack, reducing and stabilizing the bulk-pH [3].

Gaseous CO_2(g) sparging increases the cell voltage and Δp_{Base} compared to the reference experiment, probably due to the trapped gases in the stack, Fig. 5 (A, B)-red line. Upon each sparging, a spike in the voltage and Δp_{Base} curves and a sudden drop in the base-pH are seen, Fig. 5 and Fig. S9. The three downward spikes in Fig. 5 (B), at ca. 1050 s and 1500–2000 s, are due to application of a back-pressure to release possible trapped gas. As a result, part of the trapped gas probably does leave the stack as can be confirmed by a flattened curve at the same time in the voltage buildup, Fig. 5 (A)-red. The pH lowers after each 'sparge' as CO_2 lowers the pH when it is dissolved into the feed, subsequently dissolving part of the previously formed scaling, Fig. 5 (C).

However, the gaseous CO_2 sparging under the setting of Fig. 5 does not remove the scaling and even results in higher voltage and pressure-drop values compared to the reference experiment. On the bright side, increasing the CO_2(g) concentration in the stack by applying a longer

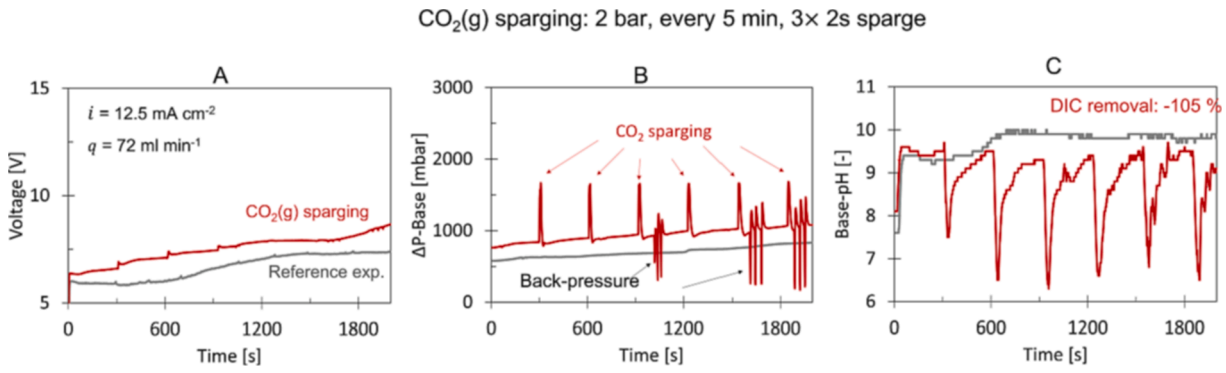

Fig. 5. Gaseous CO_2 sparging regimes for fouling removal in the CEM-BPM configuration. (A) The total cell voltage, (B) pressure drop over the base compartments, and (C) bulk-pH in the outlet from the base compartment versus time with regards to the reference experiment (i.e., no cleaning method, grey line) are shown.

sparging time of 30 s (instead of 3× 2 s) and a 3 bar-CO_2(g) pressure (instead of 2 bar), cleans the stack significantly even under accelerated scaling condition, Figure S9. However, in practice, applying longer sparging times and higher gas pressures are less economical due to the higher amount of CO_2(g) that is needed.

The CO_2(g) sparging does not (fully) recover the initial BPMED-performance and it even results in a negative DIC removal. When using CO_2(g)-sparging, the scaling buildup rate is equal or worse compared to the reference case. Furthermore, as the negative DIC removal goes against the main function of the BPMED-based oceanic carbon reduction, and because CO_2(g) sparging does not recover the stack conditions, it is ruled out for scaling removal for this technology.

As for other methods of cleaning with carbon dioxide, CO_2 (aq) saturated water cleaning for fouling mitigation has been shown effective for microfiltration (MF), ultrafiltration (UF), nanofiltration (NF), reverse osmosis (RO), electrodialysis (ED), and reverse electrodialysis (RED) [19,59]. However, in the BPMED stack, the injection of the demi-water saturated with (dissolved) CO_2 (aq) as fouling removal still does not recover the pressure drop of the AEM-BPM configuration nor decreases the irreversible voltage drops, Figure S11.

4.5. Temporary increase of the flow rate: Purge flow

Higher flow rates lead to higher velocity gradients which leads to higher wall shear stresses [60,61], often cleaning the surface fouling through physical cleaning in membrane stacks [41,54,57]. In general, places in the stack compartments where the flow velocity is low (e.g., in spacer knits) are also reported to be more prone to fouling [51,62]. A high flow velocity enhances mixing in the compartments, reducing the thickness of the diffusion boundary layer (proportional to the flow velocity ($v^{1/3}$) if Reynolds number < 1000), possibly lowering voltage-losses [62,63]. However, a sudden temporary increase in the flow rate of the BPMED-stack does not recover the cell voltage and Δp_{Base} compared to the reference experiment, Fig. 6.

In the first half of the experiments, application of the sudden-flow rate-increase does not change the cell voltage time development compared to that of the reference experiment with no cleaning. For the second half (as the scaling inside the stack increases), the pump "priming" seems to even increase the cell-voltage slightly (ca. 10 %), Fig. 6 (A). This difference is possibly resulted from various factors working against or in favor of increasing the cell voltage. With fouling present in the stack, random flow channels can form (Figure S13), resulting in a non-uniform flow velocity throughout the compartment. In RED, such nonuniform distribution of feed water increases the non-ohmic resistance due to depletion of ions (in zones where the velocity is lower [51]), increasing the cell voltage. In the BPMED case, channel formation can speed up scaling deposition because in zones with low velocity, OH^- ions concentrations can increase (given the current density is uniform), causing locally high base-pH. Such higher base-pH accelerates (the thermodynamic and kinetics of) precipitation of hydroxide/carbonate containing minerals [3]. Upon such initial precipitation, the energy barrier for further deposition of e.g., Ca^{2+}, Mg^{2+}, CO_3^{2-} or OH^- ions will decrease, enhancing the growth of the precipitates even more [64], accelerating the scaling in whole. We hypothesize the latter to be the cause of increase in the cell voltage upon "priming" the pumps. As for Δp_{Base}, no significant differences between the cases exist, except that the higher flow rates create momentary spikes of high Δp_{Base} which is expected. Mathematically, Δp increases with linear velocity v in laminar flow regime $Re_h < 1000$ [53,65]. Finally, at the end of the experiment, it seems like Δp_{Base} for 15× flow rate is slightly higher than the other two cases (ca. 150–200 mbar vs the reference case), which can confirm the above hypothesis of the accelerated fouling in high base-pH under a temporary high flow rate.

4.6. Application of back-pressure

During application of a back-pressure, the outflow is temporarily interrupted, which causes a pressure buildup inside the stack. Applying a back-pressure can decelerate fouling buildup because the flow rate is suddenly increased (more sudden than when priming) upon re-opening the outlet. In the experiments, applying a back-pressure decelerates the buildup rate of voltage and pressure drop slightly (by 20 % and 100 %, respectively), Fig. 7(A-B).

Upon closing the valve, Δp_{Base} becomes almost zero as the flow is temporarily stopped, Fig. 7 (B). After re-opening the valve, Δp_{Base} increases substantially due to the temporarily high flow flushing out of the stack (spikes in Fig. 7 (B)). The application of the back-pressure partially removes the scaling probably by mechanically removing the scaling due to the (temporary) very high flow rate (and thus high shear force [57]) that it induces upon reopening the valve. However, cleaning via applying a back-pressure does not fully restore the stack performance, and hence is not sufficient as scaling removal method. Back-pressure might be effective in combination with other scaling removal methods.

4.7. Acid wash: HCl vs BPMED-produced acid

Acid wash for fouling removal was applied in several modes including synthetic HCl solution vs acid produced by the BPMED, and

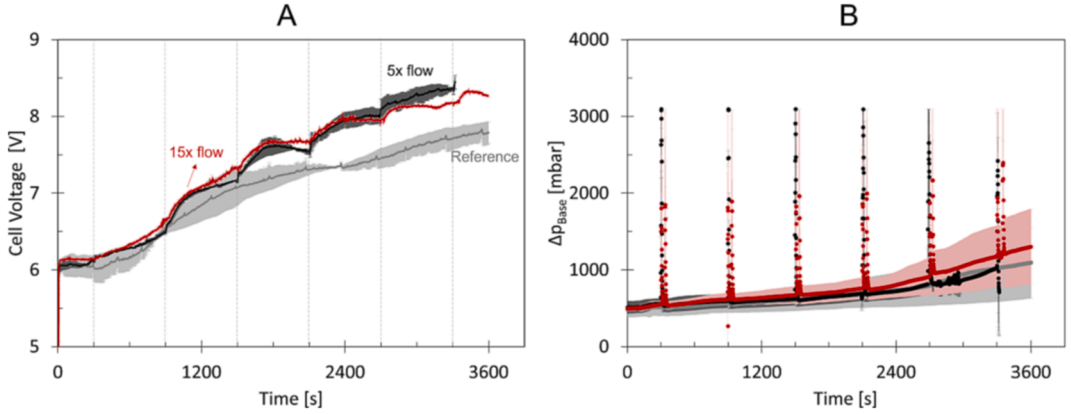

Fig. 6. Development of the (A) cell voltage and (B) Δp_{Base} with time vs the reference experiment (i.e., no cleaning method applied, grey line). All experiments were conducted for BPM-CEM, under $i = 12.5$ mAcm^{-2} and flow rate of $q = 72$ mlmin^{-1} per compartment. A sudden short flow rate increases of 5× (black) and 15× (red), applied every 10 min (for 3–5 s using the pump "prime" option), are compared (vertical grid lines in (A) indicate the purging intervals). The error bars show the standard error between two repetitions with the dark lines showing the average of two repetitions. The standard errors for the reference experiment and the experiments with 5× flow, and 15× flow is shown in light grey, dark grey and pink, respectively.

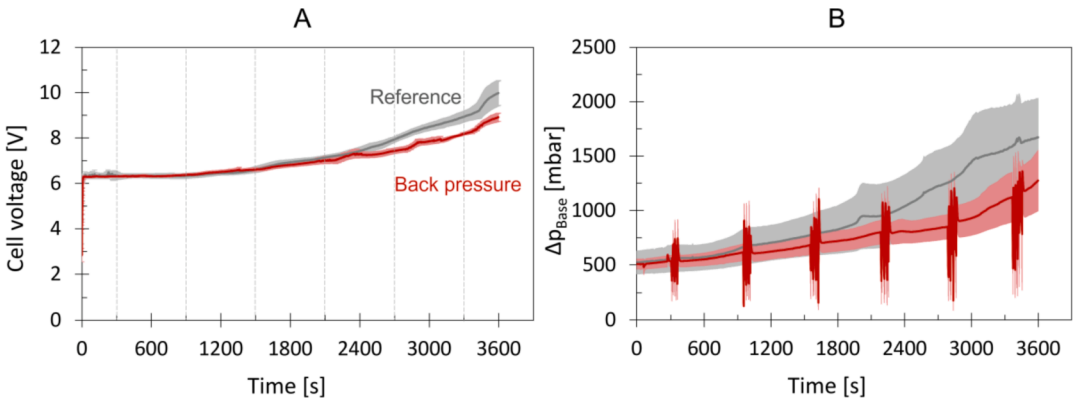

Fig. 7. Comparison of (A) the cell total voltage and (B) pressure drop vs time with the reference experiment (i.e., no cleaning method, grey line). All lines are averaged for two repetitions with back-pressure (i.e., red lines) being applied every 10 min for 3× 5 s (with stack maximum pressure of ca. 3 bar reached upon closing the valve). A stack with cell configuration of + CCBCBCBC-, under $i = 12.5$ mAcm^{-2} and flow rate of $q = 72$ mlmin^{-1} per compartment is used. The spikes in (B) show the sudden outburst of flow upon opening the valve. The error bars show the standard error of the two repetitions.

acid flow rate ranging between 0 and 200 mlmin^{-1}. In all acid wash cleaning experiments, the base-pH and the pressure drop in the base compartment decrease upon the wash, Fig. 8 and Fig. S12.

Upon the acid wash, base-pH decreases, enabling the scaling dissolution and thus fouling removal. As a result, Δp_{Base} recovers to its initial value. In Fig. 8 (A), the initial Δp_{Base} at the beginning of the experiment is 500 mbar, and after the acid wash (of ca. 15 min) Δp_{Base} becomes 590 mbar, showing > 80 % recovery, suggesting a very effective cleaning.

As for the reproducibility of data over multiple cycles, it must be noted that even under the same stack and process parameters, the location and amount of scaling, and thus the development of Δp_{Base} are not identical (Figure S12 vs 8), but all show almost full recovery upon a HCl-acid wash. It can also be seen that the Δp_{Base} increases much more steeply in Figure S12 compared to 2 (B), even though the process parameters are identical. Such a difference might be due to e.g., the spacers aging which can alter their physical form, affecting the scaling rate. To ensure optimal cleaning, the cleaning time needs to be adjusted for each case individually. The required time for the acid wash and the amount of moles of H^+ ions needed vs the pressure -recovery are compared for AEM-BPM and CEM-BPM configurations in Fig. 9.

In general, the pressure drop recovery for the AEM-BPM increases with the moles H^+ ions used (Fig. 9 (A)-orange area); this is logical as "more H^+ used" reduces the base-pH more, enhancing the scaling dissolution. "Moles of H^+ ions used" is calculated via "cleaning time × acid flow rate × H^+ ions concentration of the used acid". The scaling removal with HCl acid delivers a higher Δp_{Base} recovery (by 20 – 40 % difference) in a two to three times shorter time scale compared to the BPM-produced acid, Fig. 9 (A, B)-red vs blue bullets. These differences are probably due to the presence of various ions (e.g., Ca^{2+} and Mg^{2+} and DIC) in the BPM-produced acid that hinders the mineral dissolution and creates spots of high concentration (i.e., high mineral saturation index). Higher ionic composition/concentration increases the cleaning time and decreases the removal efficiency.

The slightly higher efficiency of the HCl acid in scaling removal compared to the BPMED-acid can (also) be due to its lower pH (pH 1.5 vs 2.4), which translates into ca. eight times higher H^+ ions concentration in the HCl acid.

Both tested acids enable chemical cleaning by dissolving the scaling. Increasing the acid flow should also contribute to an enhanced physical cleaning due to the higher shear force it creates [57]. This is confirmed as $q = 144$ mlmin^{-1} HCl wash delivers 20 % higher Δp_{Base}-recovery compared to the 72 mlmin^{-1} HCl-wash, Fig. 9 (A)-orange area. However, for the BPMED-acid, the opposite holds where a higher flow velocity v (i.e., flow rate) worsens the cleaning slightly compared to the two times lower v.

Scale formation is a multi-step complex process that involves nucleation, adhesion, and growth as explained below [66,67]. This complexity is reflected in different studies where contradictory results of higher scaling rates have been observed both in systems with increased and reduced fluid velocities [68–75]. Theoretically, the flow velocity (v) has a double effect on surface fouling [76], affecting the fouling deposition rate (i.e., proportional with the flow velocity) and its removal rate. The fouling factor (in heat exchangers) is reported to be more sensitive to the flow velocity at low flow velocities with the sensitivity decreasing by increasing the flow velocity [75]. This is observed in BPMED, as well [77]. From another point, in many studies over membrane bio-film, a

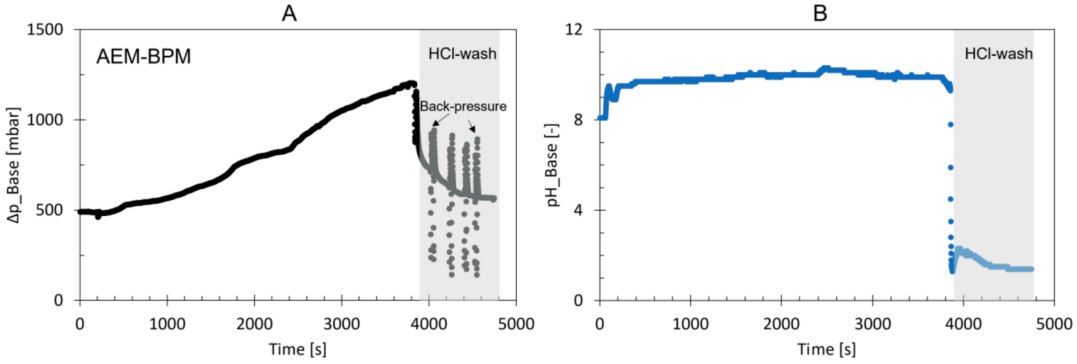

Fig. 8. Development of the pressure drop (A) and base-pH (B) prior and during an acid wash for AEM-BPM configuration, using hydrochloric acid HCl with pH 1.5 and a flow rate of $q = 72$ mlmin^{-1} per compartment for the scaling removal. The stack was 'scaled' the first hour under $i = 12.5$ mAcm^{-2} applied current density and $q = 72$ mlmin^{-1} per compartment. After 3600 s, the current is turned off. Acid wash starts (at 3864 s). Spikes during the acid wash show application of back-pressure.

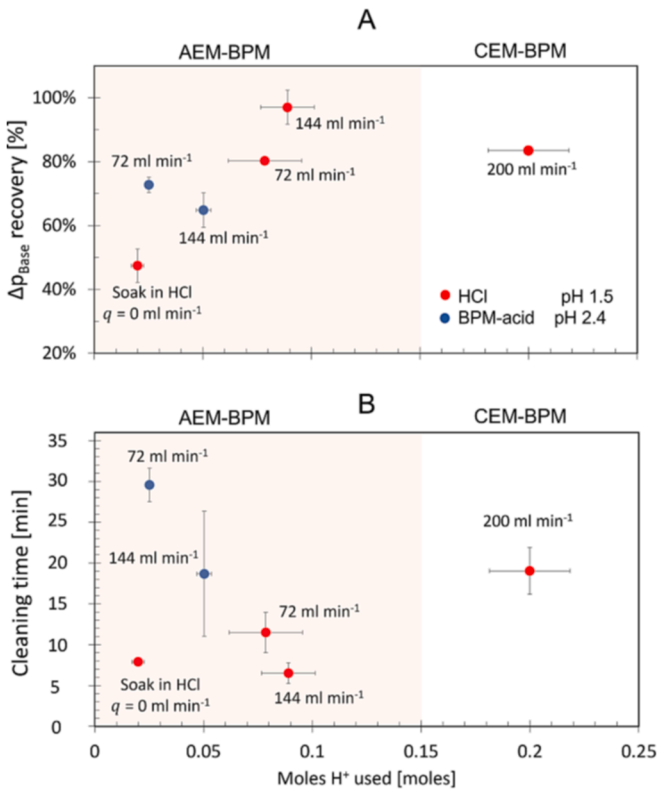

Fig. 9. (A) Recovery of the stack pressure drop and (B) cleaning time required to achieve the shown pressure recovery upon acid wash vs the amount of moles H^+ needed during the cleaning for the AEM-BPM (orange area) and BPM-CEM stack (white area). The cleaning time was noted when Δp stabilized and would not decrease with time any further. Results are the average of two repetitions and the error bars show the standard errors between the repetitions.

high hydrodynamic shear stresses makes the bio-film denser and thus more difficult to remove [78–81], which could also be the case for scaling here. We hypothesize that the effect of the higher DIC, Ca^{2+}, Mg^{2+} ions concentration of BPMED-produced-acid on hindering the mineral dissolution (and/or mineral compacting) overshadows the positive effect of a higher shear force for cleaning the scaling (i.e., detaching from the surface of the membrane/mesh-spacer) [67]. This explains why a higher flow rate in the case of the BPM-acid lowers Δp_{Base} recovery instead of improving it, Fig. 9.

When comparing the HCl with BPM-acid for the AEM-BPM (Fig. 9 (A)-red vs blue markers), the gain in Δp_{Base} recovery in case of the HCl is not much higher than the latter. However, $>2\times$ the amount of H^+ ions is needed for cleaning with HCl compared to the BPM-acid. This can be clearly seen for q 72 mlmin^{-1}, where 80 % Δp_{Base}-recovery using HCl vs 73 % using BPM-produced-acid are obtained, while the amount of moles of H^+ ions used are 0.08 vs 0.025, respectively. Furthermore, while no external chemicals/costs are associated with using the BPM-produced acid, the HCl solution needs to be either bought separately or be produced with an additional BPMED stack, increasing the costs. An alternative for minimizing the required HCl volume is "soaking the stack in HCl", which means filling the base compartments with HCl and leaving the pumps off, allowing time for mineral dissolution; if so, ca. 50 % of the scaling buildup is cleaned using the minimum amount of H^+ ions (Fig. 9 (A)), lowering the chemical costs compared to the other cases.

As for the CEM-BPM, to achieve the same Δp_{Base}-recovery, more than twice higher H^+ ions are needed compared to the AEM-BPM. This is due to the (much) higher scaling buildup in the CEM-BPM stack (Fig. 9 (A)-white area), as explained under Fig. 2.

To put the required H^+ moles for scaling cleaning in perspective, both configurations extract ca. 81 ± 1 % of the input DIC, resulting in production of ca. 0.023 mol $CaCO_3$(s) after 60 min of experiment (based on three base compartments). This is unfortunately the same number of moles as the amount of H^+ required for cleaning via e.g., the "soak HCl" or BPM-acid 72 mlmin^{-1} in Fig. 9 (A). Hence, a more efficient use of the acid-wash should be studied in future work. On the bright side, it must be noted that the cleaning here is done for the stack under accelerated scaling conditions of high current density of 12.5 mAcm^{-2} (with $q = 72$ mlmin^{-1}). This is while using similar flow rate, but a lower current density of e.g., 5 mAcm^{-2} is already shown adequate for creating the required base-pH for DIC-extraction [3]. We expect that, using the same flow rate, the experiment under 5 mAcm^{-2} should be able to be executed for at least $\frac{12.5}{5} = 2.5$ times longer than that of 12.5 mAcm^{-2}, before scaling removal is needed.

Furthermore, as the electrical energy consumption (thus voltage) has a much higher contribution to the final energy consumption than the pressure losses (Equation (1) and Figure S4), the cleaning is required mainly when the cell voltage is increased (and not necessarily the pressure drop). It is shown in Fig. 2, that the cell voltage does not increase for the AEM-BPM for ca. 2 hr even under the accelerated scaling condition of 15 mAcm^{-2}. In the worst-case scenario that the AEM-BPM cell voltage does increase drastically after 6 hr of experiment under 5 mAcm^{-2}, the required H^+ moles needed for cleaning is ≤ 17 % of the produced $CaCO_3$(s), making the cleaning step much more feasible.

5. Conclusion

This work investigates the fouling management scenarios to remove the Ca^{2+} and Mg^{2+} based scaling in the alkaline compartments of the *in-situ* bipolar membrane electrodialysis for oceanic carbon capture. The scaling buildup is measured indirectly through monitoring the increase in the total stack voltage and pressure drop (in the alkaline compartments; Δp_{Base}). The rate of scaling buildup slows down by a (continuously) higher feed flow rate in combination with lower current density, due to the lower base-pH that lowers the hydroxide precipitation kinetics. Controlling the $i - t_r$ combination in such a way that the required base-pH for carbonate extraction is reached, but hydroxide containing minerals are avoided, is an efficient fouling control strategy. As for the membrane configuration, the stack voltage for the CEM-BPM configuration increases 130 % within 30 min, while that of AEM-BPM remains constant for longer time, revealing beneficially lower scaling potential for the AEM. Air sparging, CO_2(g) sparging, CO_2(aq) saturated water cleaning, backpressure, flow rate increase (5× and 15×), and acid wash (i.e., HCl solution and BPMED-based produced acid) are investigated for scaling removal. For both membrane configurations, the acid wash showed the highest recovery. The acid wash using the BPM-produced acid (i.e., acidic seawater) needs no additional chemicals and is thus more sustainable than cleaning with HCl solution. Cleaning with HCl results in a (slightly) higher recovery and shorter cleaning time. The back-pressure as a solo method is not effective enough for fouling removal but helps decreasing the scaling rate. Air sparging increase the cell voltage and pressure drop even more because of stagnant bubbles that got trapped within the stack -spacers. CO_2(g) sparging show suppression of the voltage and pressure drop increase (even though no full recovery is achieved) but causes negative DIC-removals. We show that, for *in-situ* BPMED-based carbonate mineralization from seawater, an AEM-BPM based stack operated under current density-flow rate combination that prevents $pH_{Base} > 10$ in the base compartment is desired. For scaling removal, an acid wash is the most effective method.

Declaration of Competing Interest

The authors declare the following financial interests/personal relationships which may be considered as potential competing interests: The first and last author are co-founder of start-up company SeaO2.

Data availability

Data will be made available on request.

Acknowledgements

This work was performed in the NWO-cooperation framework of Wetsus, Centre of Excellence for Sustainable Water Technology (www.wetsus.nl). Wetsus is funded by the Dutch Ministry of Economic Affairs, the European Union Regional Development Fund, the Province of Friesland, the City of Leeuwarden and the EZ/Kompas program of the "Samenwerkingsverband Noord-Nederland". The authors like to thank the participants of the research theme "Concentrates" in Wetsus and research group "Transport phenomena" in faculty of applied sciences at TU Delft for the discussions and their (financial) support. This research received funding from the Netherlands Organization for Scientific Research (NWO) in the framework of the project ALW.2016.004.

Appendix A. Supplementary data

Supplementary data to this article can be found online at https://doi.org/10.1016/j.cej.2023.141407.

References

[1] J. Rogelj, et al., Paris Agreement climate proposals need a boost to keep warming well below 2 °c, Nature 534 (7609) (2016) 631–639.
[2] A. G. Fane, "A grand challenge for membrane desalination: More water, less carbon," *Desalination*, vol. 426, no. September 2017, pp. 155–163, 2018.
[3] R. Sharifian, L. Boer, R.M. Wagterveld, D.A. Vermaas, Oceanic carbon capture through electrochemically induced in situ carbonate mineralization using bipolar membrane, Chem. Eng. J. 438 (2022), 135326.
[4] S. El-Manharawy, A. Hafez, Study of seawater alkalization as a promising RO pretreatment method, Desalination 153 (1) (2003) 109–120.
[5] R. Sharifian, R.M. Wagterveld, I.A. Digdaya, C. Xiang, D.A. Vermaas, Electrochemical carbon dioxide capture to close the carbon cycle, Energy Environ. Sci. 14 (2) (2021) 781–814.
[6] T. Altmann, R. Das, Process improvement of sea water reverse osmosis (SWRO) and subsequent decarbonization, Desalination 499 (2021), 114791.
[7] N. Harlev, A. Bogler, O. Lahav, M. Herzberg, Acidification and decarbonization in seawater: Potential pretreatment steps for biofouling control in SWRO membranes, Desalination 467 (2019) 86–94.
[8] E. Al-Dhubhani, R. Pärnamäe, J.W. Post, M. Saakes, M. Tedesco, Performance of five commercial bipolar membranes under forward and reverse bias conditions for acid-base flow battery applications, J. Memb. Sci. 640 (2021), 119748.
[9] R. Pärnamäe, et al., Bipolar membranes: A review on principles, latest developments, and applications, J. Memb. Sci. 617 (2021), 118538.
[10] R. Sharifian, M.A. Blommaert, M. Bremer, R.M. Wagterveld, D.A. Vermaas, Intrinsic bipolar membrane characteristics dominate the effects of flow orientation and external pH-profile on the membrane voltage, J. Memb. Sci. (2021), 119686.
[11] S. Mikhaylin, L. Bazinet, Fouling on ion-exchange membranes: Classification, characterization and strategies of prevention and control, Adv. Colloid Interface Sci. 229 (2016) 34–56.
[12] C.Y. Tang, T.H. Chong, A.G. Fane, Colloidal interactions and fouling of NF and RO membranes: A review, Adv. Colloid Interface Sci. 164 (1) (2011) 126–143.
[13] C. Bellona, M. Marts, J.E. Drewes, The effect of organic membrane fouling on the properties and rejection characteristics of nanofiltration membranes, Sep. Purif. Technol. 74 (1) (2010) 44–54.
[14] B. Mi, M. Elimelech, Organic fouling of forward osmosis membranes: Fouling reversibility and cleaning without chemical reagents, J. Memb. Sci. 348 (1) (2010) 337–345.
[15] V. Parida, H.Y. Ng, Forward osmosis organic fouling: Effects of organic loading, calcium and membrane orientation, Desalination 312 (2013) 88–98.
[16] K.O. Agenson, T. Urase, Change in membrane performance due to organic fouling in nanofiltration (NF)/reverse osmosis (RO) applications, Sep. Purif. Technol. 55 (2) (2007) 147–156.
[17] G. Amy, Fundamental understanding of organic matter fouling of membranes, Desalination 231 (1) (2008) 44–51.
[18] J.S. Vrouwenvelder, C. Picioreanu, J.C. Kruithof, M.C.M. van Loosdrecht, Biofouling in spiral wound membrane systems: Three-dimensional CFD model based evaluation of experimental data, J. Memb. Sci. 346 (1) (2010) 71–85.
[19] J. Moreno, N. de Hart, M. Saakes, K. Nijmeijer, CO2 saturated water as two-phase flow for fouling control in reverse electrodialysis, Water Res. 125 (2017) 23–31.
[20] D.A. Vermaas, D. Kunteng, M. Saakes, K. Nijmeijer, Fouling in reverse electrodialysis under natural conditions, Water Res. 47 (3) (2013) 1289–1298.
[21] D. Pintossi, M. Saakes, Z. Borneman, K. Nijmeijer, Electrochemical impedance spectroscopy of a reverse electrodialysis stack: A new approach to monitoring fouling and cleaning, J. Power Sources 444 (2019), 227302.
[22] R.S. Kingsbury, F. Liu, S. Zhu, C. Boggs, M.D. Armstrong, D.F. Call, O. Coronell, Impact of natural organic matter and inorganic solutes on energy recovery from five real salinity gradients using reverse electrodialysis, J. Memb. Sci. 541 (2017) 621–632.
[23] E.J. Bodner, M. Saakes, T. Sleutels, C.J.N. Buisman, H.V.M. Hamelers, The RED Fouling Monitor: A novel tool for fouling analysis, J. Memb. Sci. 570–571 (2019) 294–302.
[24] B. Vital, E.V. Torres, T. Sleutels, M.C. Gagliano, M. Saakes, H.V.M. Hamelers, Fouling fractionation in reverse electrodialysis with natural feed waters demonstrates dual media rapid filtration as an effective pre-treatment for fresh water, Desalination 518 (2021), 115277.
[25] D.A. Vermaas, D. Kunteng, J. Veerman, M. Saakes, K. Nijmeijer, Periodic Feedwater Reversal and Air Sparging As Antifouling Strategies in Reverse Electrodialysis, Environ. Sci. Technol. 48 (5) (Mar. 2014) 3065–3073.
[26] S.A. Shah, S.-Y. Choi, S. Cho, M. Shahbabaei, R. Singh, D. Kim, Modified single-wall carbon nanotube for reducing fouling in perfluorinated membrane-based reverse electrodialysis, Int. J. Hydrog. Energy TA - TT - 45 (55) (2020) 30703–30719.
[27] T. Rijnaarts, J. Moreno, M. Saakes, W.M. de Vos, K. Nijmeijer, Role of anion exchange membrane fouling in reverse electrodialysis using natural feed waters, Colloids surfaces A Physicochem. Eng. Asp. 560 (2019) 198–204.
[28] C. Casademont, M.A. Farias, G. Pourcelly, L. Bazinet, Impact of electrodialytic parameters on cation migration kinetics and fouling nature of ion-exchange membranes during treatment of solutions with different magnesium/calcium ratios, J. Memb. Sci. 325 (2) (2008) 570–579.
[29] A.A. Moya, Uphill transport in improved reverse electrodialysis by removal of divalent cations in the dilute solution: A Nernst-Planck based study, J. Memb. Sci. 598 (2020), 117784.
[30] J. Moreno, V. Díez, M. Saakes, K. Nijmeijer, Mitigation of the effects of multivalent ion transport in reverse electrodialysis, J. Memb. Sci. 550 (2018) 155–162.
[31] Y. Zhao, J. Wang, Z. Ji, J. Liu, X. Guo, J. Yuan, A novel technology of carbon dioxide adsorption and mineralization via seawater decalcification by bipolar membrane electrodialysis system with a crystallizer, Chem. Eng. J. 381 (8) (2020), 122542.
[32] C.-F. de Lannoy, M.D. Eisaman, A. Jose, S.D. Karnitz, R.W. DeVaul, K. Hannun, J.L. B. Rivest, Indirect ocean capture of atmospheric CO2: Part I. Prototype of a negative emissions technology, Int. J. Greenh. Gas Control 70 (2018) 243–253.
[33] M. Haddad, S. Mikhaylin, L. Bazinet, O. Savadogo, J. Paris, Electrochemical acidification of Kraft black liquor by electrodialysis with bipolar membrane: Ion exchange membrane fouling identification and mechanisms, Journal of Colloid and Interface Science 488 (2017) 39–47.
[34] Y.W. Berkessa, Q. Lang, B. Yan, S. Kuang, D. Mao, L.i. Shu, Y. Zhang, Anion exchange membrane organic fouling and mitigation in salt valorization process from high salinity textile wastewater by bipolar membrane electrodialysis, Desalination 465 (2019) 94–103.
[35] Q. Wang, P. Yang, W. Cong, Cation-exchange membrane fouling and cleaning in bipolar membrane electrodialysis of industrial glutamate production wastewater, Sep. Purif. Technol. 79 (1) (2011) 103–113.
[36] H. Ren, Q. Wang, X. Zhang, R. Kang, S. Shi, W. Cong, Membrane fouling caused by amino acid and calcium during bipolar membrane electrodialysis, J. Chem. Technol. Biotechnol. 83 (11) (Oct. 2008) 1551–1557.
[37] Y. Yang, X. Gao, A. Fan, L. Fu, C. Gao, An innovative beneficial reuse of seawater concentrate using bipolar membrane electrodialysis, J. Memb. Sci. 449 (2014) 119–126.
[38] N. Pismenskaya *et al.*, "A Review on Ion-Exchange Membranes Fouling during Electrodialysis Process in Food Industry, Part 2: Influence on Transport Properties and Electrochemical Characteristics, Cleaning and Its Consequences," *Membranes*, vol. 11. p. 811.
[39] M. Szczygiełda, K. Prochaska, Effective separation of bio-based alpha-ketoglutaric acid from post-fermentation broth using bipolar membrane electrodialysis (EDBM) and fouling analysis, Biochem. Eng. J. 166 (2021), 107883.
[40] V. Kravtsov, I. Kulikova, S. Mikhaylin, L. Bazinet, Alkalinization of acid whey by means of electrodialysis with bipolar membranes and analysis of induced membrane fouling, J. Food Eng. 277 (2020), 109891.
[41] V. S. Nichka, T. R. Geoffroy, V. Nikonenko, and L. Bazinet, "Impacts of Flow Rate and Pulsed Electric Field Current Mode on Protein Fouling Formation during Bipolar Membrane Electroacidification of Skim Milk," *Membranes*, vol. 10. p. 200.
[42] F. Lin Teng Shee, J. Arul, S. Brunet, L. Bazinet, Chitosan solubilization by bipolar membrane electroacidification: Reduction of membrane fouling, J. Memb. Sci. 290 (1-2) (2007) 29–35.
[43] H. Ren, Q. Wang, X. Wu, P. Yang, W. Cong, Characterization of cation-exchange membrane fouling during bipolar membrane electrodialysis of monosodium glutamate isoelectric supernatant, J. Chem. Technol. Biotechnol. 86 (12) (Dec. 2011) 1469–1474.
[44] M.A.C.K. Hansima, et al., Fouling of ion exchange membranes used in the electrodialysis reversal advanced water treatment: A review, Chemosphere 263 (2021), 127951.
[45] J. Gilron, M. Waisman, N. Daltrophe, N. Pomerantz, M. Milman, I. Ladizhansky, E. Korin, Prevention of precipitation fouling in NF/RO by reverse flow operation, Desalination 199 (1-3) (2006) 29–30.
[46] J.W. Post, Blue Energy: electricity production from salinity gradients by reverse electrodialysis, Wageningen University and Research, 2009.
[47] H. Guo, F. You, S. Yu, L. Li, D. Zhao, Mechanisms of chemical cleaning of ion exchange membranes: A case study of plant-scale electrodialysis for oily wastewater treatment, J. Memb. Sci. 496 (2015) 310–317.
[48] D.E. Potts, R.C. Ahlert, S.S. Wang, A critical review of fouling of reverse osmosis membranes, Desalination 36 (3) (1981) 235–264.

[49] A.T.K. Tran, N. Jullok, B. Meesschaert, L. Pinoy, B. Van der Bruggen, Pellet reactor pretreatment: A feasible method to reduce scaling in bipolar membrane electrodialysis, J. Colloid Interface Sci. 401 (2013) 107–115.
[50] J. Veerman, M. Saakes, S.J. Metz, G.J. Harmsen, Reverse electrodialysis: Evaluation of suitable electrode systems, J. Appl. Electrochem. 40 (8) (2010) 1461–1474.
[51] D.A. Vermaas, M. Saakes, K. Nijmeijer, Early detection of preferential channeling in reverse electrodialysis, Electrochim. Acta 117 (2014) 9–17.
[52] A.H. Haidari, S.G.J. Heijman, W.G.J. van der Meer, Effect of spacer configuration on hydraulic conditions using PIV, Sep. Purif. Technol. 199 (2018) 9–19.
[53] G. Schock, A. Miquel, Mass transfer and pressure loss in spiral wound modules, Desalination 64 (1987) 339–352.
[54] O. Le Berre and G. D, "Skimmilk crossflow microfiltration performance versus permeation flux to wall shear stress ratio," vol. 117, pp. 261–270, 1996.
[55] K. R. Goode, K. Asteriadou, P. T. Robbins, and P. J. Fryer, "Fouling and Cleaning Studies in the Food and Beverage Industry Classified by Cleaning Type.".
[56] Y. Wibisono, Two-phase flow for fouling control in membranes, University of Twente, 2014.
[57] W. Zhang, L. Ding, M.Y. Jaffrin, B. Tang, Membrane cleaning assisted by high shear stress for restoring ultrafiltration membranes fouled by dairy wastewater, Chem. Eng. J. 325 (2017) 457–465.
[58] E. Seran, M. Godefroy, E. Pili, N. Michielsen, S. Bondiguel, What we can learn from measurements of air electric conductivity in 222Rn-rich atmosphere, Earth Sp. Sci. 4 (2) (2017) 91–106.
[59] E.R. Cornelissen, J.S. Vrouwenvelder, S.G.J. Heijman, X.D. Viallefont, D. Van Der Kooij, L.P. Wessels, Periodic air/water cleaning for control of biofouling in spiral wound membrane elements, J. Memb. Sci. 287 (1) (2007) 94–101.
[60] Y. Son, Determination of shear viscosity and shear rate from pressure drop and flow rate relationship in a rectangular channel, Polymer (Guildf) 48 (2) (2007) 632–637.
[61] D.F. Elger, B.A. LeBret, C.T. Crowe, J.A. Roberson, Engineering fluid mechanics, John Wiley & Sons, 2020.
[62] D.A. Vermaas, M. Saakes, K. Nijmeijer, Enhanced mixing in the diffusive boundary layer for energy generation in reverse electrodialysis, J. Memb. Sci. 453 (2014) 312–319.
[63] D.A. Vermaas, S. Wiegman, T. Nagaki, W.A. Smith, Ion transport mechanisms in bipolar membranes for (photo)electrochemical water splitting, Sustain. Energy Fuels 2 (9) (2018) 2006–2015.
[64] K.L. Mercer, Y.-P. Lin, P.C. Singer, Enhancing calcium carbonate precipitation by heterogeneous nucleation during chemical softening, Journal - American Water Works Association 97 (12) (2005) 116–125.
[65] B.S. Freeman, Flow and Velocity, McGraw-Hill Education, New York, NY, 2014.
[66] A. Yi-Tsung Lu, A.T. Kan, M.B. Tomson, Nucleation and Crystallization Kinetics of Barium Sulfate in the Hydrodynamic Boundary Layer: An Explanation of Mineral Deposition, Cryst. Growth Des. 21 (3) (2021) 1443–1450.
[67] I.A. Løge, J.R. Bentzon, C.G. Klingaa, J.H. Walther, B.U. Anabaraonye, P.L. Fosbøl, Scale attachment and detachment: The role of hydrodynamics and surface morphology, Chem. Eng. J. 430 (2022), 132583.
[68] A. Quddus, I.M. Allam, BaSO4 scale deposition on stainless steel, Desalination 127 (3) (2000) 219–224.
[69] M.M. Vazirian, T.V.J. Charpentier, M. de Oliveira Penna, A. Neville, Surface inorganic scale formation in oil and gas industry: As adhesion and deposition processes, J. Pet. Sci. Eng. 137 (2016) 22–32.
[70] X. Xing, C. Ma, Y. Chen, Mechanism of calcium carbonate scale deposition under subcooled flow boiling conditions, Chinese J. Chem. Eng. 13 (4) (2005) 464.
[71] A. Janzen, E.Y. Kenig, Understanding and analysis of fouling behavior of bare-wire heating elements in electric water heating, Heat Exchanger Fouling and Cleaning (2019) 1–8.
[72] M. Pourbozorg, T. Li, A.W.K. Law, Effect of turbulence on fouling control of submerged hollow fibre membrane filtration, Water Res. 99 (2016) 101–111.
[73] G.M. Graham, L.S. Boak, C.M. Hobden, Examination of the effect of generically different scale inhibitor species (PPCA and DETPMP) on the adherence and growth of barium sulphate scale on metal surfaces. In *International Symposium on Oilfield Scale*, 2001.
[74] D. Yang, J. Liu, E. Xiaoxue, L. Jiang, Model for seawater fouling and effects of temperature, flow velocity and surface free energy on seawater fouling, Chinese J. Chem. Eng. 24 (5) (2016) 658–664.
[75] Z. Han, Z. Xu, X. Yu, CFD modeling for prediction of particulate fouling of heat transfer surface in turbulent flow, Int. J. Heat Mass Transf. 144 (2019), 118428.
[76] M.M. Awad, Impact of flow velocity on surface particulate fouling-theoretical approach, J. Am. Sci. 8 (9) (2012) 442–449.
[77] V. S. Nichka and V. V Nikonenko, "Fouling Mitigation by Optimizing Flow Rate and Pulsed Electric Field during Bipolar Membrane Electroacidification of Caseinate Solution," 2021.
[78] W.K. Kwok, C. Picioreanu, S.L. Ong, M.C.M. Van Loosdrecht, W.J. Ng, J.J. Heijnen, Influence of biomass production and detachment forces on biofilm structures in a biofilm airlift suspension reactor, Biotechnol. Bioeng. 58 (4) (1998) 400–407.
[79] M.O. Pereira, M. Kuehn, S. Wuertz, T. Neu, L.F. Melo, Effect of flow regime on the architecture of a Pseudomonas fluorescens biofilm, Biotechnol. Bioeng. 78 (2) (2002) 164–171.
[80] S. Wäsche, H. Horn, D.C. Hempel, Influence of growth conditions on biofilm development and mass transfer at the bulk/biofilm interface, Water Res. 36 (19) (2002) 4775–4784.
[81] J. Vrouwenvelder, J. Kruithof, Biofouling of spiral wound membrane systems, Iwa Publishing (2011).